



HAL
open science

Low Barrier Methyl Internal Rotations and 14 N Quadrupole Coupling in the Microwave Spectrum of 2,4-Dimethylthiazole

Safa Khemissi, Vinh Van, Martin Schwell, Isabelle Kleiner, Ha Vinh Lam
Nguyen

► **To cite this version:**

Safa Khemissi, Vinh Van, Martin Schwell, Isabelle Kleiner, Ha Vinh Lam Nguyen. Low Barrier Methyl Internal Rotations and 14 N Quadrupole Coupling in the Microwave Spectrum of 2,4-Dimethylthiazole. *Journal of Physical Chemistry A*, 2023, 127 (28), pp.5779-5789. 10.1021/acs.jpca.3c01008 . hal-04246259

HAL Id: hal-04246259

<https://hal.science/hal-04246259v1>

Submitted on 17 Oct 2023

HAL is a multi-disciplinary open access archive for the deposit and dissemination of scientific research documents, whether they are published or not. The documents may come from teaching and research institutions in France or abroad, or from public or private research centers.

L'archive ouverte pluridisciplinaire **HAL**, est destinée au dépôt et à la diffusion de documents scientifiques de niveau recherche, publiés ou non, émanant des établissements d'enseignement et de recherche français ou étrangers, des laboratoires publics ou privés.

Low Barrier Methyl Internal Rotations and ^{14}N Quadrupole Coupling in the Microwave Spectrum of 2,4-Dimethylthiazole

Safa Khemissi,^{a*} Vinh Van,^b Martin Schwell,^a Isabelle Kleiner,^c and Ha Vinh Lam Nguyen^{a,d*}

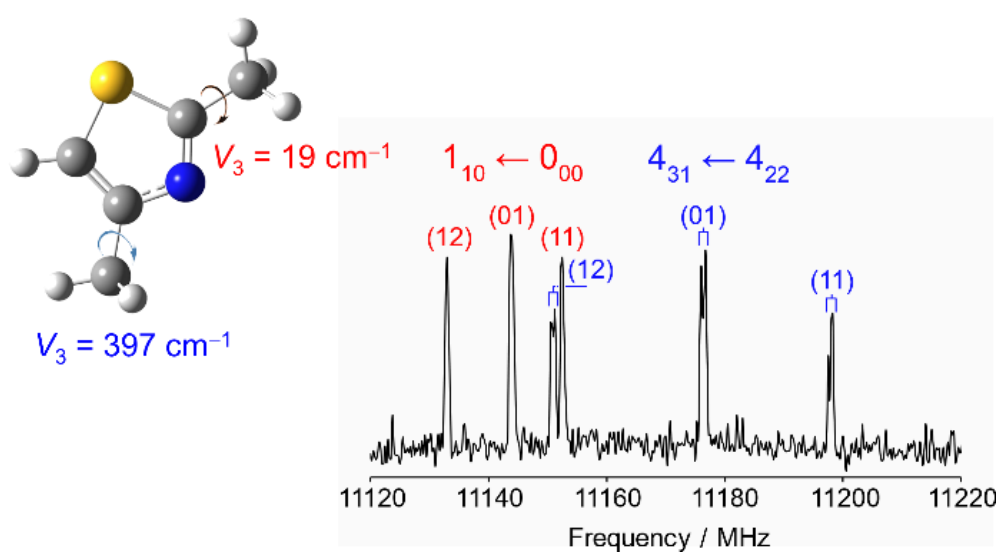
^a Univ Paris Est Creteil and Université Paris Cité, CNRS, LISA, F-94010 Créteil, France

^b Institute of Physical Chemistry, RWTH Aachen University, Landoltweg 2, D-52074 Aachen, Germany

^c Université Paris Cité and Univ Paris Est Creteil, CNRS, LISA, F-75013 Paris, France

^d Institut Universitaire de France (IUF), F-75231 Paris, France

GRAPHICAL ABSTRACT



ABSTRACT

The microwave spectrum of 2,4-dimethylthiazole was recorded using a pulsed molecular jet Fourier transform microwave spectrometer operating in the frequency range from 2.0 to 26.5 GHz. Torsional splittings into quintets were observed for all rotational transitions due to internal rotations of two inequivalent methyl groups. Hyperfine structures arising from the nuclear quadrupole coupling of the ^{14}N nucleus were fully resolved. The microwave spectra were analyzed using the modified version of the *XIAM* code and the *BELGI-C_s-2Tops-hyperfine* code. The barriers to methyl internal rotation of the 4- and 2-methyl groups were determined to be $396.707(25) \text{ cm}^{-1}$ and $19.070(58) \text{ cm}^{-1}$, respectively. The very low barrier hindering the 2-methyl torsion was a challenge for the spectral analysis and modeling, and separately fitting the five torsional species together with combination difference loops was the key for a successful assignment. The methyl torsional barriers were compared with those of other thiazole derivatives, showing the influence of the methyl group position on the barrier height. The experimental results were supported by quantum chemical calculations.

INTRODUCTION

Heterocyclic compounds form a large family of organic molecules with application in a wide range from synthetic, pharmaceutical, industrial to biological fields. Thiazole and its derivatives are among the most used aromatic five-membered heterocycles due to their structural characteristics and their various biological activities. They exist as antibacterial,¹ antiprotozoal,² and antitubercular.³ In recent years, several molecules containing a nitrogen atom have been detected in the interstellar medium (ISM), e.g. benzonitrile,⁴ 2-cyanocyclopentadiene,⁵ and cyanonaphthalene.⁶ Furthermore, a number of detected molecules exhibit methyl internal rotation(s), e.g. acetamide,⁷ methyl acetate,⁸ and methyl isocyanate.⁹

Both aspects are present in methylthiazole derivatives, increasing their chance to be detected in space. The identification of molecular lines in the ISM survey depends on the availability of sufficiently accurate laboratory data that are compared to the telescope data. High-resolution spectroscopic data obtained from laboratory studies have enabled the detection of a large number of molecular species in space.^{8,10-12} While there are many investigations on aromatic heterocycle exhibiting one methyl internal rotation,¹³⁻¹⁷ a limited number of molecules undergoing internal rotations of two methyl groups have been reported.¹⁸ For one-top molecules, all rotational lines appear as A-E doublets. In the spectra of molecules with two equivalent or inequivalent methyl tops, the lines split into quartets or quintets, respectively.¹⁹ In addition, ¹⁴N nuclear quadrupole coupling causes hyperfine splittings due to the nuclear spin $I = 1$ of the nitrogen nucleus coupled with the molecular angular momentum \mathbf{J} . The spectral assignment and modeling are more challenging for molecules combining the quadrupole hyperfine structures and the methyl internal rotation fine splittings.

The barrier hindering a methyl internal rotation is a characteristic parameter for this large amplitude motion. It is sensitive to the electrostatic and steric surrounding of the methyl group and thus varies strongly in different molecules. Generally, the barrier can take values from 0 cm^{-1} to about 1000 cm^{-1} , where values larger than about 600 cm^{-1} are considered high, lower than 200 cm^{-1} low, and in between intermediate. As shown in Figure 1, in 4- and 5-methylthiazole, intermediate torsional barriers of 358 cm^{-1} and 332 cm^{-1} , respectively, were obtained,^{20,21} but a very low barrier was found for 2-methylthiazole (35 cm^{-1}).²² Moving to 4,5-dimethylthiazole, low torsional barriers were observed for the two neighboring methyl groups (127 cm^{-1} and 62 cm^{-1} for the 4- and the 5-methyl groups, respectively) despite of steric hindrance.²³ This is most probably due to the transfer of electronic effects through the entire π -conjugated system. The electronic contribution can come from distant electronic sources, as in the case of 4-methyl-5-vinylthiazole, where the π -conjugated system of the aromatic ring

extended by the vinyl double bond impacts the methyl internal rotation, yielding a low torsional barrier of 107 cm^{-1} .²⁴ The barrier height varies in a wide range from very low (35 cm^{-1}) to intermediate (358 cm^{-1}) without any trend.

In the present work, the second member of the dimethylthiazole family, 2,4-dimethylthiazole (24DMTA), was studied using a combination of microwave spectroscopy and quantum chemical calculations with the focus on internal rotations of two inequivalent methyl groups and the nuclear quadrupole coupling effects arising from the ^{14}N nucleus.

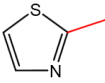
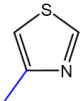
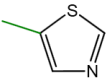
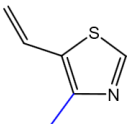
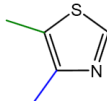

						
	(1)	(2)	(3)	(4)	(5)	(6)
V_3 / cm^{-1}	35	358	332	107	127 / 62	397 / 19
χ_{cc} / MHz	2.390	2.539	2.711	2.554	2.580	2.275

Figure 1. Comparison of the internal rotation barriers of the two methyl groups and the ^{14}N nuclear quadrupole coupling constant (NQCC) χ_{cc} in 24DMTA with the values of other thiazole derivatives. **(1)** 2-methylthiazole,²² **(2)** 4-methylthiazole,²⁰ **(3)** 5-methylthiazole,²¹ **(4)** 4-methyl-5-vinylthiazole,²⁴ **(5)** 4,5-dimethylthiazole,²³ and **(6)** 2,4-dimethylthiazole (this work).

The internal rotation effects arising from two methyl groups combined with one ^{14}N quadrupole coupling can be treated with the program *XIAM*,²⁵ where the nuclear quadrupole interactions are considered using first-order perturbation method. However, *XIAM* often struggles to reproduce and model the experimental data to the measurement accuracy for molecules with low torsional barriers^{23,26–28} due to the limited number of available parameters. In many cases, the program *BELGI-C_s-2Tops*²⁹ has shown its ability for treating such internal rotations.^{23,29–31} To model the microwave spectrum of 24DMTA, the modified version of the *XIAM* code^{32,33} and the *BELGI-C_s-2Tops-hyperfine* code²³ were used.

THEORETICAL METHODS

Geometry optimizations. Since thiazole is a planar aromatic heterocycle³⁴ and the rotations of the two methyl groups do not generate different conformers, only one conformer of 24DMTA is possible. Full geometry optimizations were performed using the *GAUSSIAN 16*³⁵ package with the B3LYP-D3BJ³⁶⁻³⁹ and MP2⁴⁰ methods combined with the 6-311++G(d,p) basis set.⁴¹ These two levels of theory were chosen as they predicted reliable rotational constants close to the experimental ones for many aromatic molecules containing two methyl groups such as three isomers of the dimethylfluorobenzene family,⁴²⁻⁴⁴ 2,5-dimethylthiophene,⁴⁵ 2,5-dimethylfuran,⁴⁶ and 2-acetyl-4-methylthiophene.⁴⁷ The optimized structure of 24DMTA is shown in Figure 2 in the principal axis system. The predicted rotational constants and dipole moment components are collected in Table 1. The atomic Cartesian coordinates are given in Table S1 in the Supporting Information. Anharmonic frequency calculations were performed to obtain ground state rotational and centrifugal distortion constants, also given in Table 1.

For benchmarking purposes, calculations using various methods combined with different Pople⁴¹ and Dunning⁴⁸ basis sets were performed to find other alternatives that can be used for thiazole derivatives or similar molecules to guide the spectral assignment. Density functional methods are B3LYP,^{36,37} including either D3,³⁸ D3BJ,³⁹ or Coulomb-attenuating method (CAM),⁴⁹ Head-Gordon's ω B97X-D,⁵⁰ Truhlar's M06-2X,⁵¹ Minnesota MN15,⁵² Perdew-Burke-Ernzerhof,⁵³ with D3 if not included in the method. The two *ab initio* methods are MP2 and coupled cluster (CCSD)⁵⁴. The predicted rotational constants are collected in Table S2 in the Supporting Information.

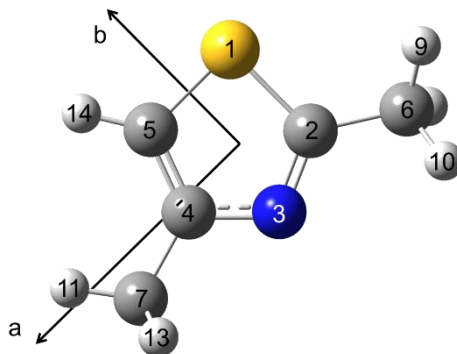


Figure 2. The optimized geometry of 24DMTA obtained at the MP2/6-311++G(d,p) level of theory in the principal axes of inertia. The nitrogen and sulfur atoms are illustrated in blue and yellow, respectively. The hydrogen atoms are white and carbon atoms are grey.

Table 1. Equilibrium rotational constants A_e , B_e , C_e , vibrational ground state rotational constants A_0 , B_0 , C_0 , quartic centrifugal distortion constants in Watson's A reduction obtained from anharmonic frequency calculations, dipole moment components in a , b , and c directions, ^{14}N nuclear quadrupole coupling constants (NQCCs) calculated at the B3LYP-D3BJ/6-311++G(d,p) and MP2/6-311++G(d,p) levels of theory.

Par.	Unit	B3LYP-D3BJ	MP2
A_e	MHz	3982.2	4022.2
B_e	MHz	1917.9	1919.1
C_e	MHz	1315.6	1320.8
A_0	MHz	3960.8	3993.7
B_0	MHz	1907.2	1907.8
C_0	MHz	1308.3	1312.2
Δ_J	kHz	0.07450	0.07440
Δ_{JK}	kHz	0.29267	0.09110
Δ_K	kHz	0.99915	1.18312
δ_J	kHz	0.02398	0.02420
δ_K	kHz	-0.22621	0.08899
$ \mu_a $	D	0.25	0.30
$ \mu_b $	D	0.75	1.15
$ \mu_c $	D	0.00	0.04
χ_{aa}	MHz	1.6795	1.5717
χ_{bb}	MHz	-4.0873	-3.7891
χ_{cc}	MHz	2.4078	2.2174
χ_{ab}	MHz	1.0729	0.8669
χ_{ac}	MHz	0.0012	0.0458
χ_{bc}	MHz	-0.0034	-0.0632

¹⁴N nuclear quadrupole coupling constants. 24DMTA contains a nitrogen atom with a nuclear spin $I = 1$, resulting in hyperfine splittings of all rotational lines which are characterized by the NQCCs. To calculate NQCC values, Bailey's method⁵⁵ was used because it has yielded reliable results for related aromatic five-membered rings, e.g., 4,5-dimethylthiazole,²³ 4-methyl-5-vinylthiazole,²⁴ 2,5-dimethylpyrrole,⁵⁶ and 2-methylpyrrole.¹⁶ Single point electronic field gradient calculation was performed at the B3PW91/6-311+G(d,p) level of theory from the structure optimized at the MP2/6-311++G(d,p) level (but other levels can be used also). The calibration factor $eQ/h = -4.599$ MHz a.u.⁻¹ was used as recommended for π -conjugated systems.⁵⁷ The calculated values of the NQCCs are $\chi_{aa} = 1.70092$ MHz, $\chi_{bb} = -3.83094$ MHz, $\chi_{cc} = 2.13002$ MHz, $\chi_{ab} = 0.87166$ MHz, $\chi_{ac} = 0.04881$ MHz, and $\chi_{bc} = -0.06051$ MHz. As no symmetry constraints were imposed during the geometry optimizations, the resulting structure did not achieve a perfect C_s symmetry, which explains the non-zero values for the two nuclear quadrupole coupling constants χ_{ac} and χ_{bc} . For comparison, we also performed electronic field gradient tensor calculations using the B3PW91/6-311+G(d,p)//B3LYP-D3BJ/6-311++G(d,p) combination and the same calibration factor. The respective value of the NQCCs constants are $\chi_{aa} = 1.62706$ MHz, $\chi_{bb} = -3.84828$ MHz, $\chi_{cc} = 2.22122$ MHz, $\chi_{ab} = 1.01653$ MHz, $\chi_{ac} = 0.00114$ MHz and $\chi_{bc} = -0.00311$ MHz.

Methyl internal rotations. 24DMTA contains two inequivalent methyl groups undergoing internal rotations. The torsional barriers of the 4-methyl and the 2-methyl groups were calculated by varying the two dihedral angles $\alpha_1 = \angle(\text{C}_5, \text{C}_4, \text{C}_7, \text{H}_{11})$ and $\alpha_2 = \angle(\text{S}_1, \text{C}_2, \text{C}_6, \text{H}_9)$, respectively, in 10° steps, while all other geometry parameters were optimized at the B3LYP-D3BJ/6-311++G(d,p) and MP2/6-311++G(d,p) levels. Due to the three-fold symmetry of the methyl groups, a rotation of 120° was sufficient. The obtained energy points were parameterized with a Fourier expansion with the coefficients given in Table S3 in the Supporting Information. The potential energy curves are illustrated in Figures

Figure 3 and Figure 4. For the 4-methyl group, a three-fold torsional potential was obtained at both levels, and the V_3 term of the potential was determined to be 404.4 (B3LYP-D3BJ), cm⁻¹ and 363.4 cm⁻¹ (MP2), respectively. For the 2-methyl group, the potential curve remains three-

fold in calculations at the B3LYP-D3BJ/6-311++G(d,p) level of theory with a V_3 term of 46.6 cm^{-1} and a V_6 contribution of 7.6 cm^{-1} , but with the MP2 method, the significant V_6 term of 29.8 cm^{-1} clearly dominates the V_3 term of 14.2 cm^{-1} .

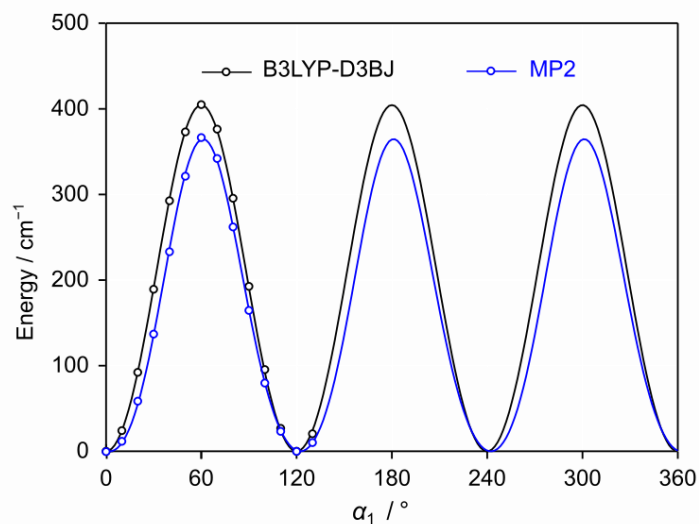


Figure 3. The potential energy curves of 24DMTA corresponding to the rotation of the 4-methyl group obtained at the B3LYP-D3BJ/6-311++G(d,p) and MP2/6-311++G(d,p) levels of theory by varying the dihedral angle $\alpha_1 = \angle(C_5, C_4, C_7, H_{11})$ in 10° steps. The calculated barrier to methyl internal rotation is 404.4 cm^{-1} for B3LYP-D3BJ (black curve) and 363.4 cm^{-1} for MP2 (blue curve). The energies are given relative to the lowest absolute energies of $E_{\text{B3LYP-D3BJ}} = -647.8089211$ Hartree and $E_{\text{MP2}} = -646.4851466$ Hartree.

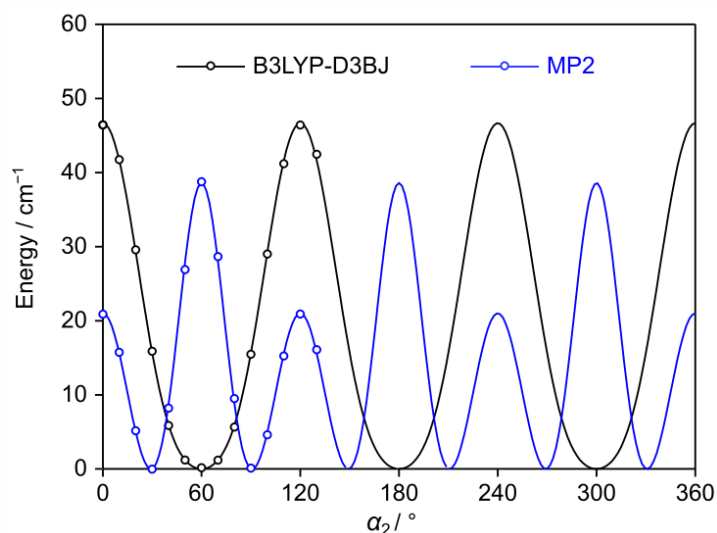


Figure 4. The potential energy curves of 24DMTA corresponding to the rotation of the 2-methyl group obtained at the B3LYP-D3BJ/6-311++G(d,p) and MP2/6-311++G(d,p) levels of theory by varying the dihedral angle $\alpha_2 = \angle(\text{S}_1, \text{C}_2, \text{C}_6, \text{H}_9)$ in 10° steps. The calculated V_3 term is 46.6 cm^{-1} for B3LYP-D3BJ (black curve) and a ratio V_3/V_6 of $14.2 \text{ cm}^{-1}/29.8 \text{ cm}^{-1}$ is needed to reproduce the MP2 results (blue curve). The energies are given relative to the lowest absolute energies of $E_{\text{B3LYP-D3BJ}} = -647.8089210$ Hartree and $E_{\text{MP2}} = -646.4851484$ Hartree.

Potential energy surfaces. The two-dimensional potential energy surfaces (2D-PES) depending on the rotation of the 4- and 2-methyl groups were obtained by varying the dihedral angles $\alpha_1 = \angle(\text{C}_5, \text{C}_4, \text{C}_7, \text{H}_{11})$ and $\alpha_2 = \angle(\text{S}_1, \text{C}_2, \text{C}_6, \text{H}_9)$, respectively, in 10° steps, while all other geometry parameters were optimized. Calculations at the B3LYP-D3BJ/6-311++G(d,p) level of theory indicate that coupling between the two methyl rotors exists, as the shape of the minimum regions is oblate instead of circular which would be the observation in the absence of top-top coupling. For all data points, a maximal deviation of about 1% was obtained. At the MP2/6-311++G(d,p) level, the 2D-PES also visualizes significant coupling, which requires not only the $\cos(3\alpha_1)\cos(3\alpha_2)$ term but also the $\sin(3\alpha_1)\sin(3\alpha_2)$ term to be fitted (see Table S4 in the Supporting Information). The top-top coupling is enabled by the electronic transfer due to

the π -electronic delocalization of the double bonds of the thiazole ring. The dominant V_6 term over the V_3 term predicted for the 2-methyl torsion can be recognized by three double minimum regions of α_2 (in purple) at $\alpha_1 = 60^\circ, 180^\circ,$ and 300° , as illustrated in Figure 5.

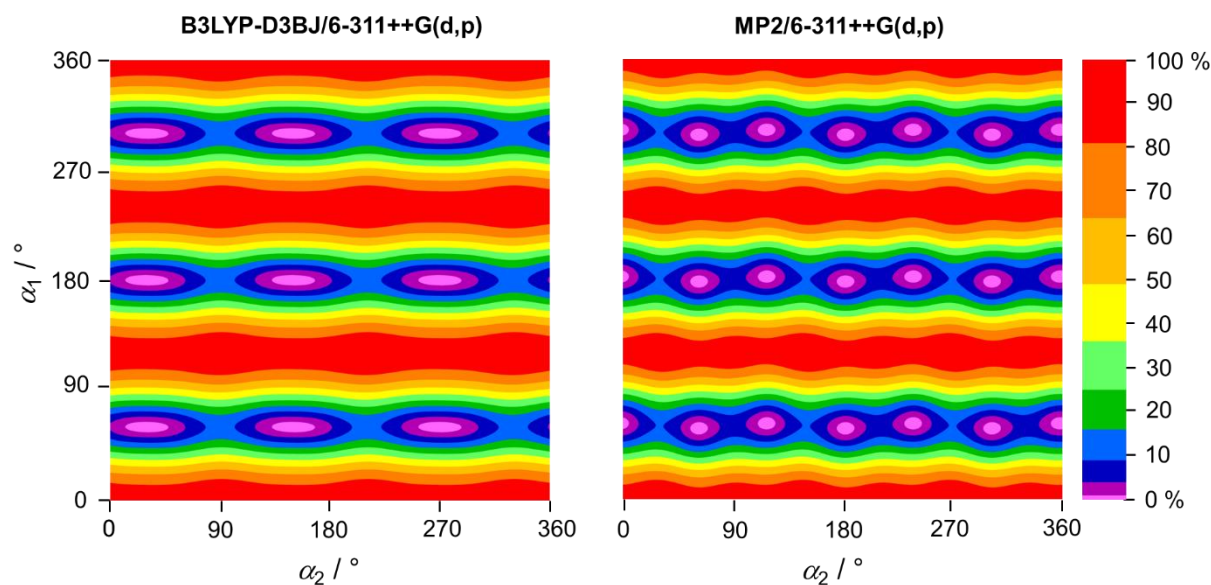


Figure 5. The 2D-PES of 24DMTA depending on the rotation of the 4- and 2-methyl groups obtained by varying the dihedral angles $\alpha_1 = \angle(\text{C}_5, \text{C}_4, \text{C}_7, \text{H}_{11})$ and $\alpha_2 = \angle(\text{S}_1, \text{C}_2, \text{C}_6, \text{H}_9)$, respectively, in 10° steps, while all other geometry parameters were optimized at the B3LYP-D3BJ/6-311++G(d,p) and MP2/6-311++G(d,p) levels of theory. The numbers in color code indicate the energy (in percent) relative to the energetic minimum (0%) and maximum (100%) with $E_{\min}(\text{B3LYP-D3BJ}) = -647.808921$, $E_{\min}(\text{MP2}) = -646.485147$ Hartree (0 %), $E_{\max}(\text{B3LYP-D3BJ}) = -647.806911$ Hartree, and $E_{\max}(\text{MP2}) = -646.483260$ Hartree (100 %). The relative energies are $\Delta E_{\text{B3LYP-D3BJ}} = 441.1 \text{ cm}^{-1}$ and $\Delta E_{\text{MP2}} = 414.1 \text{ cm}^{-1}$. Note that the scale is not linear to represent the low torsional barrier of the 2-methyl group.

EXPERIMENTAL SECTION

Measurements. The rotational spectrum of 24DMTA was recorded in the frequency range of 2.0 to 26.5 GHz using a molecular jet Fourier-transform microwave spectrometer.⁵⁸ The sample was purchased from TCI Europe, Zwijndrecht, Belgium, with a purity of 98%. A few drops of

24DMTA were put on a 6 cm piece of a pipe cleaner placed in front of the nozzle. Helium was used as carrier gas. The mixture of helium and 24DMTA was expanded into the vacuum chamber with a backing pressure of 2 bar.

A broadband scan was recorded at a step size of 0.25 MHz in the frequency range from 8.5 to 15.1 GHz. A portion of the scan from 11120 to 11220 MHz is given in Figure 6, where lines are marked with their assigned quantum numbers and torsional species. Furthermore, all lines observed in the stepped scan were re-measured at a higher resolution, appearing as Doppler doublets due to the coaxial beam-resonator arrangement. The instrumental accuracy is 2 kHz.⁵⁹ The estimated measurement accuracy for 24DMTA is about 6 kHz due to line broadening from unresolved splittings arising probably from the spin-spin and spin-rotation coupling. A typical high-resolution spectrum is given in Figure 7.

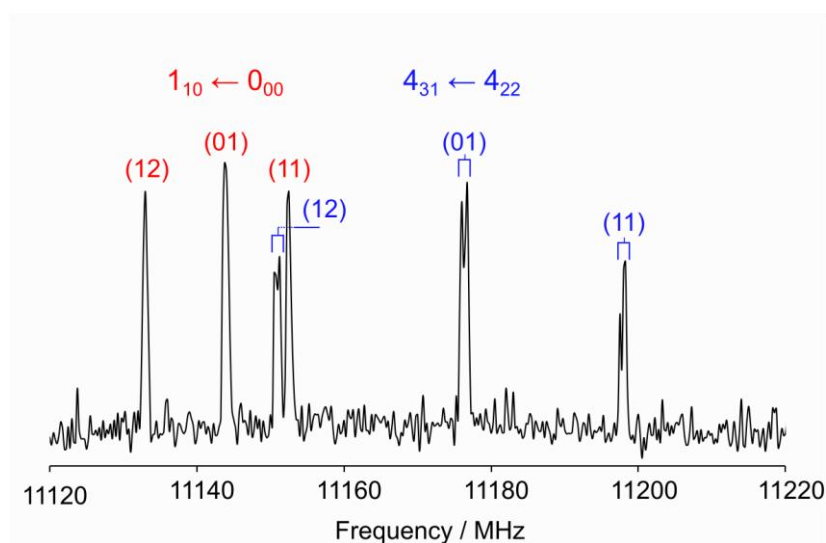


Figure 6. A portion of the broadband survey spectra of 24DMTA in the frequency range from 11120 to 11220 MHz recorded by overlapping spectra width of 0.25 MHz with 50 co-added decays per each single measurement. The arbitrary intensity is given in a logarithmic scale. All signals are marked with their assigned quantum numbers and torsional species. The splittings of the $4_{31} \leftarrow 4_{22}$ transition lines are from the ^{14}N nuclear quadrupole coupling.

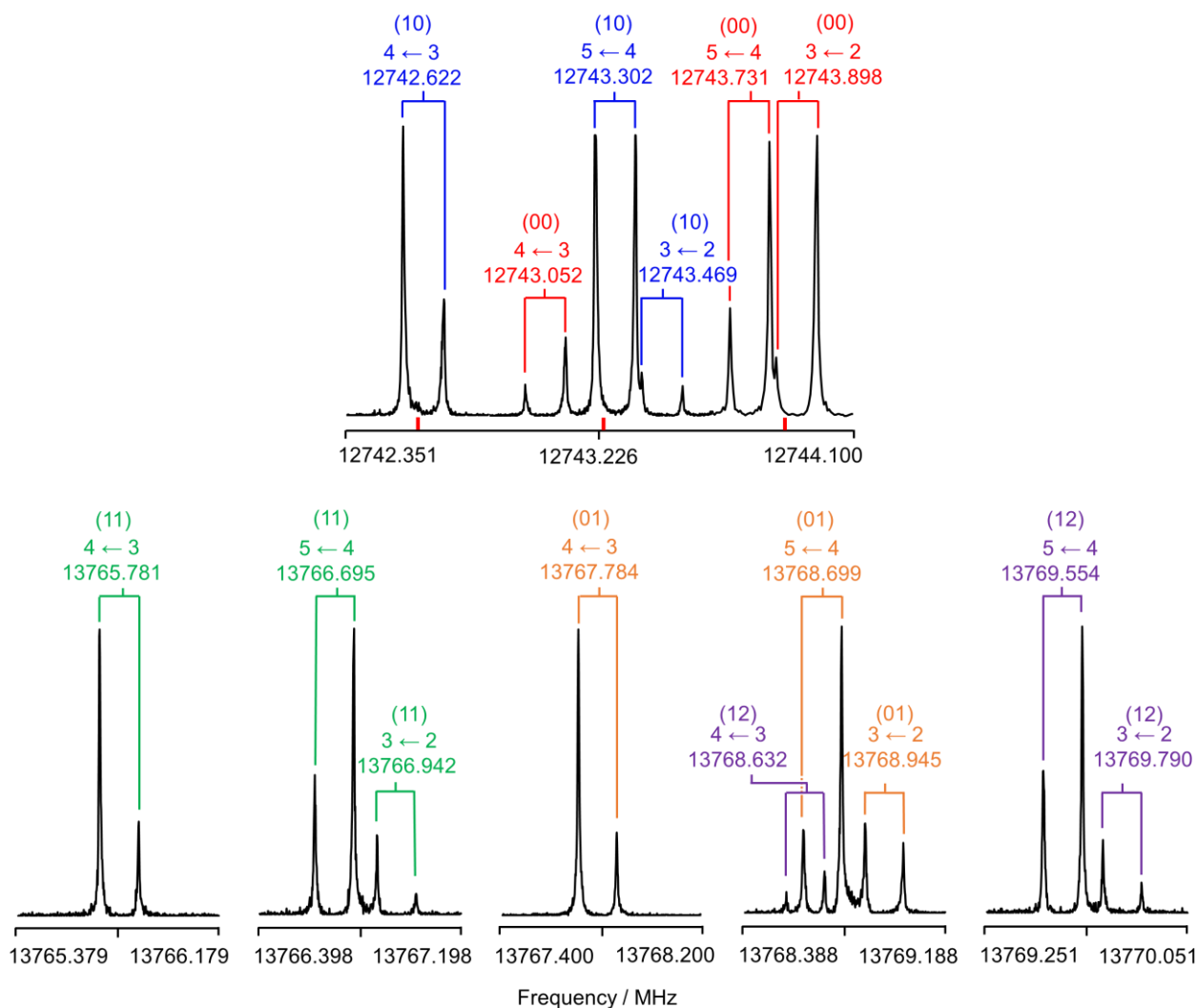


Figure 7. A typical high-resolution spectrum of the b -type transition $4_{14} \leftarrow 3_{03}$. The ^{14}N quadrupole hyperfine components are given as $F' \leftarrow F$. All the frequencies are given in MHz. The torsional species are given in parenthesis; the Doppler doubles are marked by brackets. For the spectrum shown on the upper trace, three high resolution measurements are combined. The polarization frequencies of 12742.602 MHz, 12743.251 MHz, and 12743.850 MHz are marked as red lines. For the spectra on the upper trace, 50 free induction decays were co-added. The intensities are normalized.

Spectral assignment. 24DMTA features two inequivalent methyl groups undergoing internal rotation. Due to these effects, each rotational transition splits into five torsional species called (00), (10), (01), (11), and (12),⁶⁰ each of them splits in addition due to the ^{14}N nuclear quadrupole coupling. At the beginning, 24DMTA was considered as an effective rigid rotor

(with only the (00) species), where both the methyl internal rotations and the ^{14}N quadrupole coupling effects were neglected to facilitate the spectral assignment. The theoretical rigid-rotor spectrum was predicted with the *XIAM* code²⁵ using the rotational constants and the dipole moment components calculated at the MP2/6-311++G(d,p) level of theory given in Table 1. Due to obvious planarity, only transitions of *a*- and *b*-types were expected. The predicted spectrum was compared with the broadband scan from 8.5 to 15.1 GHz. The most intense transitions with $K_a = 0, 1$, e.g., $3_{13} \leftarrow 2_{02}$, $3_{03} \leftarrow 2_{02}$, $4_{14} \leftarrow 3_{03}$, and $4_{04} \leftarrow 3_{13}$, were identified straightforwardly. As a second step, the hyperfine structures of the (00) components were assigned using the NQCCs predicted with Bailey's method, and an initial fit including 54 lines was obtained.

To investigate the two methyl internal rotations, only the internal rotation of the 4-methyl group was treated first due to its intermediate torsional barrier and the normal behavior of its potential energy curve (see Figure 3). To predict the one-top spectrum, the torsional barrier calculated at the B3LYP-D3BJ/6-311++G(d,p) level of theory and the angle between the principal *a*-axis and the methyl rotor axis taken from the structure optimized at the MP2/6-311++G(d,p) level of theory were input in the *XIAM* code. The rotational constants and NQCCs were taken from the rigid-rotor fit. The (10) species lines, including their hyperfine splittings, were found easily because the (10) and (00) components are close in frequency and can often be captured in the same high-resolution measurement, as shown in the example spectrum given in Figure 7. In total, a fit with 126 lines was obtained with $J \leq 6$ and a satisfactory standard deviation of about 4.4 kHz.

To consider the 2-methyl rotor, we expanded the one-top fit to a two-top fit by adding the corresponding torsional barrier and angle. The assignment and modeling of the (01), (11), and (12) components were challenging due to the low barrier to internal rotation and the large splittings between the torsional species. The (01) species were assigned after several attempts

first by searching for some intense *b*-type transitions, which guided later the assignment of the (11) and (12) components. A small number of weak *a*-type, but also some forbidden *c*- and *x*-type (even ΔK_a and ΔK_c) transitions were observed in the spectrum. For *c*- and *x*-type transitions, the quantum numbers K_a and K_c have no meaning and they only indicate the order of energy. During the assignment process, most *a*- and *b*-type frequencies were checked by combination difference loops (Ritz cycles)⁶¹ to ensure the correct assignment as shown in Figure 8. The hyperfine components of each rotation-torsional transition were also checked by Ritz cycles, as illustrated in Figure 9. Once the number of assigned lines became sufficiently large, each torsional species including the hyperfine splittings was fitted separately using the *WS18* code⁵⁶ where odd power order parameters in the \mathbf{H}_{op} term of the Hamiltonian^{32,61} were needed for all torsional species other than (00):

$$\mathbf{H}_{\text{op}} = (q + q_J \mathbf{P}^2 + q_K \mathbf{P}_z^2 + q_{JK} \mathbf{P}^2 \mathbf{P}_z^2 + q_{KK} \mathbf{P}_z^4) \mathbf{P}_z + (r + r_J \mathbf{P}^2 + r_K \mathbf{P}_z^2 + r_{JK} \mathbf{P}^2) \cdot \frac{1}{2} (\mathbf{P}_+ + \mathbf{P}_-). \quad (1)$$

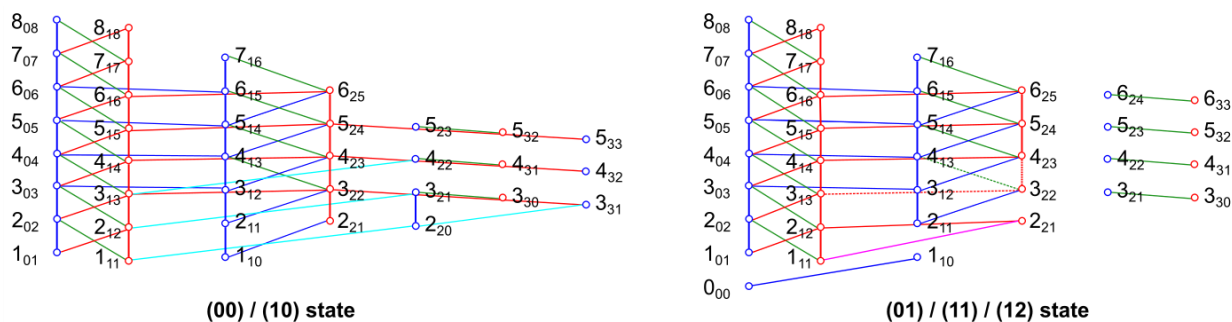


Figure 8 Schematic illustration of almost all the rotation energy levels of the (00), (10), (01), (11), and (12) torsional species of 24DMTA. Solid lines connecting the circles indicate transitions that were checked by combination differences loops. Hyperfine components are considered (see Figure 9), though the loops shown here only indicate the rotation-torsional transitions. Many of the loops sum within 2 kHz, but there are also some loops which sum to 10-20 kHz. Taking the average of all loop sums, the

estimated measurement accuracy is 6 kHz. A number of weak *a*-type transitions could not be measured. Therefore, some loops are not closed. Transitions involving in such loops are indicated as dashed lines.

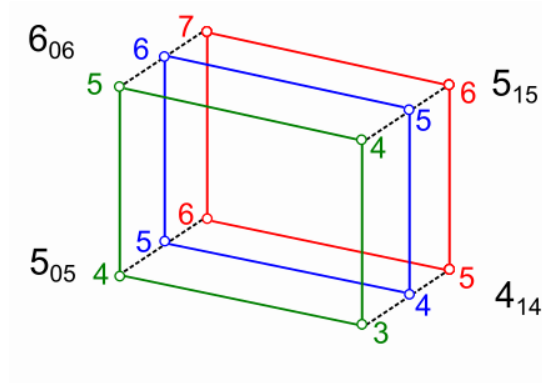


Figure 9 Schematic illustration of three Ritz cycles used to checked the hyperfine components. The numbers in black indicate the quantum numbers of the rotational transitions $J_{K_a K_c}$. The numbers in red, blue, and green are the quantum numbers F . The hyperfine components of the same rotational level are connected by the dashed black lines to ease the reading.

The separate (00), (10), (01), (11), and (12) fits given in

Table 2 possess reasonable standard deviations close to the measurement accuracy, confirming that all lines are correctly assigned. The combination of Ritz cycles and separate fits was the key to a successful assignment of the (01), (11), and (12) species.

In total, 919 lines including the hyperfine splittings resulting from the ^{14}N nuclear quadrupole coupling were fitted using a modified version of the program (*XIAM_{mod}*)^{32,33} that can fit two more parameters compared to the original version of *XIAM*, to a standard deviation of 46.0 kHz, while the measurement accuracy is estimated to be 6 kHz. To improve the quality of the global fit, the *BELGI-C_s-2Tops-hyperfine* code²³ was applied for the same data set. With more fitted molecular parameters, *BELGI-C_s-2Tops-hyperfine* succeeded to decrease the standard deviation to 6.5 kHz. The molecular parameters in the principal axis system obtained using the two programs are collected in Table 3; the fitted frequencies are listed in Table S5 in the Supporting Information. The *BELGI* parameters obtained in the “quasi-PAM” system²⁹ are given in Table 4. Only some of them can be converted into the principal axis system for a direct comparison with the *XIAM_{mod}* parameters (see Table 3). We note that the centrifugal distortion constants are contaminated by the internal rotation effects and have become effective in the Hamiltonian. Therefore, they no longer present the effect of centrifugal distortion in the *XIAM_{mod}* fit and their values differ from the predicted ones. In the separate fits shown in Table 2, all parameters are effective.

In addition to the 919 lines fitted using the two programs, four *Q*-branch transitions including their hyperfine splittings have been assigned but were excluded from the fits due to their large deviations. Their frequencies are given in the Table S6 in the Supporting Information.

Table 2. Molecular parameters used for the (00), (10), (01), (11), and (12) separate fits obtained with the *WS18* code.

Par. ^a	Unit	Fit (00)	Fit (10)	Fit (01)	Fit (11)	Fit (12)
<i>A</i>	MHz	4103.54846(22)	4103.07615(22)	4051.6945(14)	4051.2189(13)	4051.2616(13)
<i>B</i>	MHz	1930.92274(13)	1930.91066(13)	1926.70375(32)	1926.69027(32)	1926.69103(30)
<i>C</i>	MHz	1324.529750(71)	1324.529786(71)	1324.22004(34)	1324.22020(31)	1324.22107(32)
Δ_J	kHz	0.080(2)	0.079(2)	0.274(3)	0.268(2)	0.278(2)
Δ_{JK}	kHz	0.446(8)	0.399(7)	11.699(73)	11.289(51)	11.310(54)
Δ_K	kHz	2.557(16)	2.633(16)	37.67(32)	40.09(28)	39.76(26)
δ_J	kHz	0.027(1)	0.027(1)	0.123(1)	0.121(1)	0.125(1)
δ_K	kHz	0.202(22)	0.227(22)	6.254(52)	5.990(52)	6.062(52)
χ_{aa}	MHz	1.5074(14)	1.5034(14)	1.4946(20)	1.4897(17)	1.4924(15)
χ_{bb}^b	MHz	-3.7789(17)	-3.7815(17)	-3.7744(27)	-3.7717(24)	-3.7702(24)
χ_{cc}^b	MHz	2.2715(36)	2.2781(36)	2.2798(61)	2.2818(53)	2.2779(55)
χ_{ab}	MHz			0.9667(24)	0.9584(23)	0.9662(22)
<i>q</i>	MHz		10.6122(14)	5293.5343(14)	5303.1709(13)	5282.4062(14)
<i>q_K</i>	MHz		-5.17(16)	-1.53313(44)	-1.53487(39)	-1.52583(40)
<i>q_J</i>	MHz			-0.23756(16)	-0.23819(12)	-0.23771(13)
<i>q_{JK}</i>	kHz			-0.594(23)	-0.468(18)	-0.509(19)
<i>q_{KK}</i>	kHz			-0.991(82)	-1.616(81)	-1.432(73)
<i>r</i>	MHz			1568.3905(11)	1566.59567(79)	1569.88788(77)
<i>r_K</i>	MHz			-1.45909(29)	-1.45851(27)	-1.46174(25)
<i>r_J</i>	MHz			-0.042623(21)	-0.042670(21)	-0.042710(20)
<i>N</i> ^c		196	199	167	178	179
<i>rms</i> ^d	kHz	5.3	4.8	4.7	3.7	5.0

^a All molecular parameters refer to the principal axis system. Watson's A reduction in the I' representation was used. ^b Derived from $\chi_- = \chi_{bb} - \chi_{cc}$. ^c Number of lines. ^d Root-mean-square deviation of the fit.

Table 3. Molecular parameters of 24DMTA in the principal axis system obtained using the *XIAM_{mod}* and *BELGI-C_s-2Tops-hyperfine* programs.

Par. ^a	Unit	<i>XIAM_{mod}</i>	<i>BELGI</i>	Calc.
<i>A</i>	MHz	4035.2460(41)	4035.59(15)	4022.2 ^b
<i>B</i>	MHz	1925.07535(64)	1925.1714(67)	1919.1 ^b
<i>C</i>	MHz	1324.51247(55)	1324.4563(58)	1320.8 ^b
Δ_J	kHz	0.0192(63)		0.07440 ^b
Δ_{JK}	kHz	0.773(86)		0.09110 ^b
Δ_K	kHz	1.68(25)		1.18312 ^b
$V_{3,1}$	cm ⁻¹	396.707(25)	403.329(44)	363.4 ^b
$V_{3,2}$	cm ⁻¹	19.070(58)	23.2597(63)	14.2 ^b
V_{cc}	cm ⁻¹	-1.941(36)	-3.256(17)	
ρ_1	unitless	0.02423 ^c	0.024514(13)	
ρ_2	unitless	0.02231 ^c	0.0222649(19)	
F_{12}	GHz	3.06205 ^c	3.1625(86)	
$D_{p_i^2 K,1}$	MHz	-0.158(62)		
$D_{p_i^2 J,2}$	MHz	0.0501(80)		
$D_{p_i^2 K,2}$	MHz	1.517(34)		
$D_{p_i^2 -,2}$	MHz	0.165(14)		
$D_{c3J,2}$	MHz	-0.435(76)		
$D_{c3K,2}$	MHz	-8.68(37)		
$D_{c3-,2}$	MHz	-1.17(13)		
$\angle(i_1,a)$	deg	18.403(23)	18.127(15)	16.3 ^b
$\angle(i_1,b)$	deg	108.403(23)	108.127(15)	106.3 ^b
$\angle(i_1,c)$	deg	90.00 ^d	90.00 ^d	90.2 ^b
$\angle(i_2,a)$	deg	147.9662(3)	147.7669(67)	148.0 ^b
$\angle(i_2,b)$	deg	122.0338(3)	122.2331(67)	121.9 ^b
$\angle(i_2,c)$	deg	90.00 ^d	90.00 ^d	88.5 ^b
χ_{aa}	MHz	1.483(16)	1.4849(23)	1.70092 ^e
χ_{bb}^f	MHz	-3.758(21)	-3.7612(20)	-3.83094 ^e
χ_{cc}^f	MHz	2.275(45)	2.2763(30)	2.13002 ^e
$ \chi_{ab} $	MHz	0.963(29)	0.9873(42)	0.87166 ^e
N^g		919	919	
rms^h	kHz	46.0	6.5	

^a All parameters refer to the principal axis system. Watson's A reduction in the I' representation was used. ^b Calculated at the MP2/6-311++G(d,p) level of theory. The rotational constants refer to the equilibrium structure. The centrifugal distortion constants are obtained from anharmonic frequency calculations. ^c Derived parameters in *XIAM_{mod}*. ^d Fixed due to symmetry. ^e The NQCCs calculated at the B3PW91/6-311+G(d,p)//MP2/6-311++G(d,p) levels of theory using Bailey's method (see text). ^f Derived from $\chi_- = \chi_{bb} - \chi_{cc}$. ^g Number of hyperfine components. ^h Root-mean-square deviation of the fit.

Table 4. Molecular parameters of 24DMTA in the quasi-PAM axis system obtained by *BELGI-C_s-2Tops-hyperfine*.

Operator ^a	Par. ^b	Unit	Value
\mathbf{P}_z^2	<i>A</i>	MHz	4209.44(11)
\mathbf{P}_x^2	<i>B</i>	MHz	1934.0669(53)
\mathbf{P}_y^2	<i>C</i>	MHz	1324.4563(59)
$-\mathbf{P}^4$	Δ_J	kHz	0.0596(16)
$-\mathbf{P}^2\mathbf{P}_z^2$	Δ_{JK}	kHz	-0.097(22)
$-\mathbf{P}_z^2$	Δ_K	kHz	2.003(36)
$-2\mathbf{P}^2(\mathbf{P}_x^2 - \mathbf{P}_y^2)$	δ_J	kHz	0.02008(92)
$(1/2)(1 - \cos 3\alpha_1)$	$V_{3,1}$	cm ⁻¹	403.329(44)
$\mathbf{P}_z\mathbf{p}_1$	q_1	GHz	8.0745(42)
$\mathbf{P}_x\mathbf{p}_1$	r_1	GHz	1.22696(79)
\mathbf{p}_1^2	f_1	GHz	163.9759 ^c
$(1/2)(1 - \cos 3\alpha_2)$	$V_{3,2}$	cm ⁻¹	23.2597(63)
$\mathbf{P}_z\mathbf{p}_2$	q_2	GHz	7.13496(50)
$\mathbf{P}_x\mathbf{p}_2$	r_2	GHz	-2.05036(46)
\mathbf{p}_2^2	f_2	GHz	163.5744 ^c
$\mathbf{P}_z\mathbf{p}_1\mathbf{P}^2$	q_{2J}	MHz	0.01113(72)
$\mathbf{P}_z^3\mathbf{p}_2$	q_{2K}	MHz	-0.08094(75)
$\mathbf{P}_x\mathbf{p}_1\mathbf{P}^2$	r_{2J}	kHz	3.087(28)
$(1/2)\{\mathbf{P}_z^2, \mathbf{P}_x\}\mathbf{p}_2$	r_{2K}	MHz	-0.0758(38)
$\mathbf{p}_2^2\mathbf{P}^2$	f_{2J}	MHz	-0.05705(27)
$(1 - \cos 3\alpha_1)(1 - \cos 3\alpha_2)$	V_{12C}	cm ⁻¹	-3.256(18)
$\mathbf{p}_1\mathbf{p}_2$	f_{12}	cm ⁻¹	0.21098(57)
$(1/2)(1 - \cos 3\alpha_2)\{\mathbf{P}_z, \mathbf{P}_x\}$	$V_{3,2AB}$	MHz	-6.28(23)
$(1/2)(1 - \cos 3\alpha_2)\{\mathbf{P}_x^2 - \mathbf{P}_y^2\}$	$V_{3,2BC}$	MHz	-0.0836(74)
	$2\chi_{aa}$	MHz	2.9829(45)
	$2\chi_{bb}$	MHz	-7.5355(40)
	$2\chi_{ab}$	MHz	-1.9377(83)
	N^d		919
	rms^e	kHz	6.5

^a Operator which the parameters multiply in the program. The torsional angles α_1 and α_2 correspond to the 4- and 2-methyl groups, respectively. {A, B} is the anti-commutator AB + BA. ^b All parameters refer to the quasi-PAM system. ^c Fixed to values from the *XIAM_{mod}* fit. ^d Number of torsional components including their hyperfine splittings. ^e Root-mean-square deviation of the fit.

RESULTS AND DISCUSSION

The microwave spectrum of 24DMTA was analyzed and a total of 919 rotational lines including the hyperfine splittings arising from the ^{14}N nuclear quadrupole coupling were fitted using the *XIAM_{mod}* and *BELGI-C_s-2Tops-hyperfine* programs to rms deviation of 46.0 kHz and 6.5 kHz, respectively. The estimated measurement accuracy is 6 kHz.

Rotational constants. The experimental rotational constants obtained using the *XIAM_{mod}* and *BELGI-C_s-2Tops-hyperfine* programs are in good agreement, and they also agree well with those predicted at the MP2/6-311++G(d,p) level of theory, where the deviation does not exceed 0.6 %. Results from the basis set variation (see Table S2 in the Supporting Information) show that at all levels, the differences between calculated equilibrium and experimental vibrational ground state rotational constants are reasonable with deviations being less than 2.7% for all methods/basis sets used, but Pople's basis sets often performs better than Dunning's basis sets. Therefore, calculated equilibrium rotational constants can be used to guide the spectral assignment. Particularly, the MN15/6-31G(d,p) level of theory calculated almost exactly the three constants, gives a deviation of about 0.02% for *A* rotational constant, and less than 0.4% for *B* and *C*. The B3LYP-D3BJ method combined with 6-311+G(3df,3pd) and 6-311++G(3df,3pd) basis sets predicts rotational constants closest to the experimental ones, providing a deviation less than 0.2 % for the three constants. The MP2/6-31G(d,p) level recommended for other aromatic rings^{13,47,63-67} also performs well for 24DMTA.

Inertial defect. The planarity of the thiazoles is caused by the conjugated π -electronic system for which the inertial defect Δ_c gives direct information. For planar molecules containing two methyl groups, the inertial defect is about $-6.4 \text{ u}\text{\AA}^2$.⁶⁸ The value of 24DMTA calculated using the rotational constants of the *XIAM_{mod}* fit is $-6.207 \text{ u}\text{\AA}^2$, which is almost the same as those found for other planar aromatic five-membered rings containing two methyl groups such as 4,5-methylthiazole ($-6.225 \text{ u}\text{\AA}^2$),²³ 2,5-dimethylfuran ($-6.280 \text{ u}\text{\AA}^2$),⁴⁶ and 2,5-dimethylthiophene.⁴⁵

It is also close to the values obtained for the two conformers of 2-acetyl-5-methylfuran (-6.580 u\AA^2 and -6.469 u\AA^2 for the *cis* and *trans* conformers, respectively),⁶⁹ the 3,4-isomer of dimethylbenzaldehyde (-6.469 u\AA^2 and -6.452 u\AA^2 for the *anti* and *syn* conformers, respectively),³¹ and the values calculated at the B3LYP-D3BJ and MP2/6-311++G(d,p) levels (-6.275 u\AA^2 and -6.350 u\AA^2 , respectively).

¹⁴N nuclear quadrupole coupling constants. The NQCCs values obtained with the *XIAM_{mod}* and *BELGI-C_s-2Tops-hyperfine* codes are extremely similar and are very close to the values calculated at the B3PW91/6-311+G(d,p)//MP2-311++G(d,p) levels of theory. This combination of the two levels gives excellent agreement with the experimental values for many molecules with π -conjugated system.^{23,57,70} Calculated values obtained using the B3PW91/6-311+G(d,p)//B3LYP-D3BJ/6-311++G(d,p) combination are also in good agreement with the experimental values. Bailey's method yielded sufficiently accurate results and are therefore recommended for similar substituted thiazoles.

For 24DMTA, the principal *c*-axis is collinear with one axis of the coupling tensor because they are both perpendicular to the thiazole ring plane. Therefore, the NQCC χ_{cc} can be directly compared with those obtained for other thiazole derivatives, as illustrated in Figure 1. The χ_{cc} values of 2-methylthiazole (**1**) and 24DMTA (**6**) are very similar. Almost identical values were observed for 4-methylthiazole (**2**), 4-methyl-5-vinylthiazole (**4**), and 4,5-dimethylthiazole (**5**), which are the same as the value of 2.585(11) MHz found for thiazole.⁷¹ A slightly larger value was observed for the 5-methylthiazole (**3**). This shows that the electronic surrounding of the nitrogen nucleus is not affected much if a methyl group is attached at the 4-position of the ring, while changes by a substitution at the 2 and the 5-positions are more significant.

Methyl internal rotations. The barriers to internal rotation of the 2- and 4-methyl group deduced using the *XIAM_{mod}* program are $19.070(58) \text{ cm}^{-1}$ and $396.707(25) \text{ cm}^{-1}$, respectively,

close to the values obtained with *BELGI-C_s-2Tops-hyperfine* (23.2597(63) cm⁻¹ and 403.329(44) cm⁻¹). The differences are probably due to the different fitting methods and sets of fitted parameters. For the 4-methyl rotor, the V_3 values calculated using B3LYP-D3BJ/6-311++G(d,p) and MP2/6-311++G(d,p) levels of theory differ by about 7.7 cm⁻¹ and 32.9 cm⁻¹, respectively, compared to the value to *XIAM_{mod}* fit. The respective deviations for the 2-methyl rotor are 27.5 cm⁻¹ and 4.9 cm⁻¹. However, we note that the potential barrier of the 2-methyl rotor predicted at the MP2/6-311++G(d,p) level of theory involves a V_6 contribution larger than V_3 (see Figure 4). Attempts to fit V_6 were not successful, since only rotational transitions from vibrational ground state are available in the data set.

The torsional barriers of 24DMTA were compared with values found for other thiazole derivatives shown in Figure 1. Barrier heights of the 2-methyl and the 4-methyl rotors close to those of the methyl groups in 2-methylthiazole²² and 4-methylthiazole,²⁰ respectively, were expected due to the similarity of the electronic and steric environment around each methyl group. Indeed, an intermediate potential barrier of about 397 cm⁻¹ was obtained for the 4-methyl group (**6**), only slightly larger than the values of 358 cm⁻¹ found for 4-methylthiazole (**2**).²⁰ The 2-methyl group (**6**) possesses a much lower value of about 19 cm⁻¹, close to the value of 2-methylthiazole (**1**, 35 cm⁻¹).²² The barrier increase of the 4-methyl group and the barrier decrease of the 2-methyl group could be explained by the coupling between the methyl rotors caused by the electronic transfer through the entire π -system due to π -electron delocalization, as mentioned in the potential energy surfaces section. The dramatic differences compared to 5-methylthiazole (**3**),²¹ 4-methyl-5-vinylthiazole (**4**),²⁴ 4,5-dimethylthiazole (**5**)²³ are also most probably due to electrostatic effects, as discussed in Refs. 18 and ²⁴.

CONCLUSION

The microwave spectrum of 24DMTA recorded under molecular jet conditions was successfully assigned. Five torsional species arising from two inequivalent internal rotations and the ^{14}N quadrupole hyperfine splittings were observed, the line frequencies were fitted using the *XIAM_{mod}* and *BELGI-C_s-2Tops-hyperfine* programs. Not only the assignment, but also the fitting process were challenging. The whole data set was reproduced with an rms deviation of 46.0 kHz using the *XIAM_{mod}* code. The *BELGI-C_s-2Tops-hyperfine* program succeeded to decrease the rms deviation to 6.5 kHz. An intermediate torsional barrier of $396.707(25)\text{ cm}^{-1}$ and a very low barrier of $19.070(58)\text{ cm}^{-1}$ were found for the 4-methyl and the 2-methyl groups, respectively. These values are close to those found for the corresponding monomethyl thiazoles. Comparison with other thiazole derivatives leads to the conclusion that the barriers to internal rotation are influenced by the positions of the methyl groups in the thiazole ring as well as the top-top coupling enabled by the electronic transfer due to π -electron delocalization.

ASSOCIATED CONTENT

Supporting Information. Nuclear coordinates of the optimized structure, basis set variation, Fourier coefficients of the potential curves and the 2D-PES, and frequency list.

AUTHOR INFORMATION

Corresponding author:

lam.nguyen@lisa.ipsl.fr and safa.khemissi@lisa.ipsl.fr

Authors contributions

The manuscript was written through the contributions of all authors. All authors have given approval to the final version of the manuscript.

ACKNOWLEDGMENTS

We thank Laura Hoppe Alvarez for her contribution within a student research project at the RWTH Aachen University. This work was supported by the Agence Nationale de la Recherche ANR (project ID ANR-18-CE29-0011) and by the European Union (ERC, 101040480-LACRIDO). Views and opinions expressed are however those of the authors only and do not necessarily reflect those of the European Union. Neither the European Union nor the granting authority can be held responsible for them. Part of the simulations were performed with computing resources granted by the RWTH Aachen University under project rwth0506.

REFERENCES

- (1) Oh, C.-H.; Cho, H.-W.; Baek, D.; Cho, J.-H. Synthesis and Antibacterial Activity of 1 β -Methyl-2-(5-Substituted Thiazolo Pyrrolidin-3-Ylthio)Carbapenem Derivatives. *Eur. J. Med. Chem.* **2002**, *37*, 743–754.
- (2) Tapia, R. A.; Prieto, Y.; Pautet, F.; Walchshofer, N.; Fillion, H.; Fenet, B.; Sarciron, M.-E. Synthesis and Antiprotozoal Evaluation of Benzothiazolopyrroloquinoxalinones, Analogues of Kuanoniamine A. *Bioorg. Med. Chem.* **2003**, *11*, 3407–3412.
- (3) Suresh Kumar, G. V.; Rajendraprasad, Y.; Mallikarjuna, B. P.; Chandrashekar, S. M.; Kistayya, C. Synthesis of Some Novel 2-Substituted-5-[Isopropylthiazole] Clubbed

1,2,4-Triazole and 1,3,4-Oxadiazoles as Potential Antimicrobial and Antitubercular Agents. *Eur. J. Med. Chem.* **2010**, *45*, 2063–2074.

- (4) McGuire, B. A.; Burkhardt, A. M.; Kalenskii, S.; Shingledecker, C. N.; Remijan, A. J.; Herbst, E.; McCarthy, M. C. Detection of the Aromatic Molecule Benzonitrile ($c\text{-C}_6\text{H}_5\text{CN}$) in the Interstellar Medium. *Science* **2018**, *359*, 202–205.
- (5) Lee, K. L. K.; Changala, P. B.; Loomis, R. A.; Burkhardt, A. M.; Xue, C.; Cordiner, M. A.; Charnley, S. B.; McCarthy, M. C.; McGuire, B. A. Interstellar Detection of 2-Cyanocyclopentadiene, $\text{C}_5\text{H}_5\text{CN}$, a Second Five-Membered Ring Toward TMC-1. *Astrophys. J. Lett.* **2021**, *910*, L2.
- (6) McGuire, B. A.; Loomis, R. A.; Burkhardt, A. M.; Lee, K. L. K.; Shingledecker, C. N.; Charnely, S. B.; Cooke, I. R.; Cordiner, M. A.; Herbst, E.; Kalenskii, S.; Siebert, M. A.; Willis, E. R.; Xue, C.; Remijan, A. J.; McCarthy, M. C. Detection of Two Interstellar Polycyclic Aromatic Hydrocarbons via Spectral Matched Filtering. *Science* **2021**, *371*, 1265–1269.
- (7) Hollis, J. M.; Lovas, F. J.; Remijan, A. J.; Jewell, P. R.; Ilyushin, V. V.; Kleiner, I. Detection of Acetamide (CH_3CONH_2): The Largest Interstellar Molecule with a Peptide Bond. *Astrophys. J.* **2006**, *643*, L25.
- (8) Tercero, B.; Kleiner, I.; Cernicharo, J.; Nguyen, H. V. L.; López, A.; Caro, G. M. M. Discovery of Methyl Acetate and Gauche Ethyl Formate in Orion. *Astrophys. J.* **2013**, *770*, L13.
- (9) Halfen, D. T.; Ilyushin, V. V.; Ziurys, L. M. Interstellar Detection of Methyl Isocyanate CH_3NCO in Sgr B2(N): A Link from Molecular Cloud to Comets. *Astrophys. J.* **2015**, *812*, L5.

- (10) López, A.; Tercero, B.; Kisiel, Z.; Daly, A. M.; Bermúdez, C.; Calcutt, H.; Marcelino, N.; Viti, S.; Drouin, B. J.; Medvedev, I. R.; Neese, C. F.; Pszczółkowski, L.; Alonso, J. L.; Cernicharo, J. Laboratory Characterization and Astrophysical Detection of Vibrationally Excited States of Vinyl Cyanide in Orion-KL. *Astron. Astrophys.* **2014**, *572*, A44.
- (11) Manigand, S.; Calcutt, H.; Jørgensen, J. K.; Taquet, V.; Müller, H. S. P.; Coutens, A.; Wampfler, S. F.; Ligterink, N. F. W.; Drozdovskaya, M. N.; Kristensen, L. E.; Wiel, M. H. D. van der; Bourke, T. L. The ALMA-PILS Survey: The First Detection of Doubly Deuterated Methyl Formate (CHD₂OCHO) in the ISM. *Astron. Astrophys.* **2019**, *623*, A69.
- (12) Bizzocchi, L.; Prudenzano, D.; Rivilla, V. M.; Pietropolli-Charmet, A.; Giuliano, B. M.; Caselli, P.; Martín-Pintado, J.; Jiménez-Serra, I.; Martín, S.; Requena-Torres, M. A.; Rico-Villas, F.; Zeng, S.; Guillemin, J.-C. Propargylimine in the Laboratory and in Space: Millimetre-Wave Spectroscopy and Its First Detection in the ISM. *Astron. Astrophys.* **2020**, *640*, A98.
- (13) Hakiri, R.; Derbel, N.; Nguyen, H. V. L.; Mouhib, H. Communication through the Furan Ring: The Conformational Effect on the Internal Rotation of 5-Methyl Furfural Studied by Microwave Spectroscopy. *Phys. Chem. Chem. Phys.* **2018**, *20*, 25577–25582.
- (14) Jäger, W.; Dreizler, H.; Mäder, H.; Sheridan, J.; Walls, C. T. The Microwave Spectrum of 4-Methylisoxazole: ¹⁴N Nuclear Quadrupole Coupling, Methyl Internal Rotation and Electric Dipole Moment. *Z. Naturforsch.* **1987**, *42a*, 501–506.

- (15) Nguyen, T.; Stahl, W.; Nguyen, H. V. L.; Kleiner, I. ^{14}N Nuclear Quadrupole Coupling and Methyl Internal Rotation in 3-Methylpyrrole Investigated by Microwave Spectroscopy. *J. Mol. Spectrosc.* **2020**, *372*, 111351.
- (16) Nguyen, T.; Dindic, C.; Stahl, W.; Nguyen, H. V. L.; Kleiner, I. ^{14}N Nuclear Quadrupole Coupling and Methyl Internal Rotation in the Microwave Spectrum of 2-Methylpyrrole. *Mol. Phys.* **2020**, *118*, 1668572.
- (17) Wörmke, S.; Brendel, K.; Andresen, U.; Mäder, H. A Molecular Beam Fourier Transform Microwave Study of 2-Methylpyridine and Its Complex with Argon: Structure, Methyl Internal Rotation and ^{14}N Nuclear Quadrupole Coupling. *Mol. Phys.* **2004**, *102*, 1625–1639.
- (18) Nguyen, H. V. L.; Caminati, W.; Grabow, J.-U. The LAM of the Rings: Large Amplitude Motions in Aromatic Molecules Studied by Microwave Spectroscopy. *Mol. Basel Switz.* **2022**, *27*, 3948.
- (19) Nguyen, H. V. L.; Kleiner, I. Understanding (Coupled) Large Amplitude Motions: The Interplay of Microwave Spectroscopy, Spectral Modeling, and Quantum Chemistry. *Phys. Sci. Rev.* **2020**, *7*, 679–726.
- (20) Jäger, W.; Mäder, H. The Microwave Spectrum of 4-Methylthiazole: Methyl Internal Rotation, ^{14}N Nuclear Quadrupole Coupling and Electric Dipole Moment. *Z. Naturforsch.* **1987**, *42a*, 1405–1409.
- (21) Jäger, W.; Mäder, H. The Microwave Spectrum of 5-Methylthiazole: Methyl Internal Rotation, ^{14}N Nuclear Quadrupole Coupling and Electric Dipole Moment. *J. Mol. Struct.* **1988**, *190*, 295–305.

- (22) Nguyen, T.; Van, V.; Gutlé, C.; Stahl, W.; Schwell, M.; Kleiner, I.; Nguyen, H. V. L. The Microwave Spectrum of 2-Methylthiazole: ^{14}N Nuclear Quadrupole Coupling and Methyl Internal Rotation. *J. Chem. Phys.* **2020**, *152*, 134306.
- (23) Van, V.; Nguyen, T.; Stahl, W.; Nguyen, H. V. L.; Kleiner, I. Coupled Large Amplitude Motions: The Effects of Two Methyl Internal Rotations and ^{14}N Quadrupole Coupling in 4,5-Dimethylthiazole Investigated by Microwave Spectroscopy. *J. Mol. Struct.* **2020**, *1207*, 127787.
- (24) Khemissi, S.; Schwell, M.; Kleiner, I.; Nguyen, H. V. L. Influence of π -Electron Conjugation Outside the Aromatic Ring on the Methyl Internal Rotation of 4-Methyl-5-Vinylthiazole. *Mol. Phys.* **2022**, *120*, e2052372.
- (25) Hartwig, H.; Dreizler, H. The Microwave Spectrum of Trans-2,3-Dimethyloxirane in Torsional Excited States. *Z. Naturforsch.* **1996**, *51a*, 923–932.
- (26) Ferres, L.; Stahl, W.; Nguyen, H. V. L. Conformational Effects on the Torsional Barriers in *m*-Methylanisole Studied by Microwave Spectroscopy. *J. Chem. Phys.* **2018**, *148*, 124304.
- (27) Ferres, L.; Stahl, W.; Nguyen, H. V. L. Low Torsional Barrier Challenges in the Microwave Spectrum of 2,4-Dimethylanisole. *J. Chem. Phys.* **2019**, *151*, 104310.
- (28) Ferres, L.; Truong, K.-N.; Stahl, W.; Nguyen, H. V. L. Interplay Between Microwave Spectroscopy and X-Ray Diffraction: The Molecular Structure and Large Amplitude Motions of 2,3-Dimethylanisole. *ChemPhysChem* **2018**, *19*, 1781–1788.
- (29) Tudorie, M.; Kleiner, I.; Hougen, J. T.; Melandri, S.; Sutikdja, L. W.; Stahl, W. A Fitting Program for Molecules with Two Inequivalent Methyl Tops and a Plane of

Symmetry at Equilibrium: Application to New Microwave and Millimeter-Wave Measurements of Methyl Acetate. *J. Mol. Spectrosc.* **2011**, *269*, 211–225.

- (30) Nguyen, H. V. L.; Van, V.; Stahl, W.; Kleiner, I. The Effects of Two Internal Rotations in the Microwave Spectrum of Ethyl Methyl Ketone. *J. Chem. Phys.* **2014**, *140*, 214303.
- (31) Tudorie, M.; Kleiner, I.; Jahn, M.; Grabow, J.-U.; Goubet, M.; Pirali, O. Coupled Large Amplitude Motions: A Case Study of the Dimethylbenzaldehyde Isomers. *J. Phys. Chem. A* **2013**, *117*, 13636–13647.
- (32) Herbers, S.; Nguyen, H. V. L. Next Level Achievement of the *XIAM* Code in Modeling the Microwave Spectrum of *m*-Methylanisole. *J. Mol. Spectrosc.* **2020**, *370*, 111289.
- (33) Herbers, S.; Fritz, S. M.; Mishra, P.; Nguyen, H. V. L.; Zwier, T. S. Local and Global Approaches to Treat the Torsional Barriers of 4-Methylacetophenone Using Microwave Spectroscopy. *J. Chem. Phys.* **2020**, *152*, 074301.
- (34) Esselman, B. J.; Zdanovskaia, M. A.; Owen, A. N.; Stanton, J. F.; Woods, R. C.; McMahon, R. J. Precise Equilibrium Structure of Thiazole (*c*-C₃H₃NS) from Twenty-Four Isotopologues. *J. Chem. Phys.* **2021**, *155*, 054302.
- (35) Frisch, M. J.; Trucks, G. W.; Schlegel, H. B.; Scuseria, G. E.; Robb, M. A.; Cheeseman, J. R.; Scalmani, G.; Barone, V.; Petersson, G. A.; Nakatsuji, H., et al. *Gaussian 16*, Revision B.01; Gaussian, Inc., Wallingford CT, 2016.
- (36) Becke, A. D. Density-functional Thermochemistry. III. The Role of Exact Exchange. *J. Chem. Phys.* **1993**, *98*, 5648–5652.

- (37) Lee, C.; Yang, W.; Parr, R. G. Development of the Colle-Salvetti Correlation-Energy Formula into a Functional of the Electron Density. *Phys. Rev. B* **1988**, *37* (2), 785–789.
- (38) Grimme, S.; Ehrlich, S.; Goerigk, L. Effect of the Damping Function in Dispersion Corrected Density Functional Theory. *J. Comput. Chem.* **2011**, *32*, 1456–1465.
- (39) Grimme, S.; Antony, J.; Ehrlich, S.; Krieg, H. A Consistent and Accurate Ab Initio Parametrization of Density Functional Dispersion Correction (DFT-D) for the 94 Elements H-Pu. *J. Chem. Phys.* **2010**, *132*, 154104.
- (40) Møller, C.; Plesset, M. S. Note on an Approximation Treatment for Many-Electron Systems. *Phys. Rev.* **1934**, *46*, 618–622.
- (41) Frisch, M. J.; Pople, J. A.; Binkley, J. S. Self-consistent Molecular Orbital Methods 25. Supplementary Functions for Gaussian Basis Sets. *J. Chem. Phys.* **1984**, *80*, 3265–3269.
- (42) Khemissi, S.; Nguyen, H. V. L. Two Equivalent Internal Rotations in the Microwave Spectrum of 2,6-Dimethylfluorobenzene. *ChemPhysChem* **2020**, *21*, 1682–1687.
- (43) Mélan, J.; Khemissi, S.; Nguyen, H. V. L. Steric Effects on Two Inequivalent Methyl Internal Rotations of 3,4-Dimethylfluorobenzene. *Spectrochim. Acta. A.* **2021**, *253*, 119564.
- (44) Khemissi, S.; Pérez Salvador, A.; Nguyen, H. V. L. Large Amplitude Motions in 2,3-Dimethylfluorobenzene: Steric Effects Failing to Interpret Hindered Methyl Torsion. *J. Phys. Chem. A* **2021**, *125*, 8542–8548.

- (45) Van, V.; Stahl, W.; Nguyen, H. V. L. Two Equivalent Methyl Internal Rotations in 2,5-Dimethylthiophene Investigated by Microwave Spectroscopy. *Phys. Chem. Chem. Phys.* **2015**, *17*, 32111–32114.
- (46) Van, V.; Bruckhuisen, J.; Stahl, W.; Ilyushin, V.; Nguyen, H. V. L. The Torsional Barriers of Two Equivalent Methyl Internal Rotations in 2,5-Dimethylfuran Investigated by Microwave Spectroscopy. *J. Mol. Spectrosc.* **2018**, *343*, 121–125.
- (47) Dindić, C.; Barth, M.; Nguyen, H. V. L. Two Methyl Internal Rotations of 2-Acetyl-4-Methylthiophene Explored by Microwave Spectroscopy and Quantum Chemistry. *Spectrochim. Acta A* **2022**, *280*, 121505.
- (48) Dunning, T. H. Gaussian Basis Sets for Use in Correlated Molecular Calculations. I. The Atoms Boron through Neon and Hydrogen. *J. Chem. Phys.* **1989**, *90*, 1007–1023.
- (49) Yanai, T.; Tew, D. P.; Handy, N. C. A New Hybrid Exchange-Correlation Functional Using the Coulomb-Attenuating Method (CAM-B3LYP). *Chem. Phys. Lett.* **2004**, *393* (1), 51–57.
- (50) Chai, J.-D.; Head-Gordon, M. Long-Range Corrected Hybrid Density Functionals with Damped Atom-Atom Dispersion Corrections. *Phys. Chem. Chem. Phys.* **2008**, *10*, 6615–6620.
- (51) Zhao, Y.; Truhlar, D. G. The M06 Suite of Density Functionals for Main Group Thermochemistry, Thermochemical Kinetics, Noncovalent Interactions, Excited States, and Transition Elements: Two New Functionals and Systematic Testing of Four M06-Class Functionals and 12 Other Functionals. *Theor. Chem. Acc.* **2008**, *120*, 215–241.

- (52) Yu, H. S.; He, X.; Li, S. L.; Truhlar, D. G. MN15: A Kohn–Sham Global-Hybrid Exchange–Correlation Density Functional with Broad Accuracy for Multi-Reference and Single-Reference Systems and Noncovalent Interactions. *Chem. Sci.* **2016**, *7*, 5032–5051.
- (53) Adamo, C.; Barone, V. Toward Reliable Density Functional Methods without Adjustable Parameters: The PBE0 Model. *J. Chem. Phys.* **1999**, *110*, 6158–6170.
- (54) Bartlett, R. J.; Musiał, M. Coupled-Cluster Theory in Quantum Chemistry. *Rev. Mod. Phys.* **2007**, *79*, 291–352.
- (55) Bailey, W. C. DFT and HF–DFT Calculations of ^{14}N Quadrupole Coupling Constants in Molecules. *Chem. Phys.* **2000**, *252*, 57–66.
- (56) Nguyen, T.; Stahl, W.; Nguyen, H. V. L.; Kleiner, I. Local vs Global Approaches to Treat Two Equivalent Methyl Internal Rotations and ^{14}N Nuclear Quadrupole Coupling of 2,5-Dimethylpyrrole. *J. Chem. Phys.* **2021**, *154*, 204304.
- (57) Kannengießer, R.; Stahl, W.; Nguyen, H. V. L.; Bailey, W. C. ^{14}N Quadrupole Coupling in the Microwave Spectra of N-Vinylformamide. *J. Mol. Spectrosc.* **2015**, *317*, 50–53.
- (58) Grabow, J.; Stahl, W.; Dreizler, H. A Multioctave Coaxially Oriented Beam-resonator Arrangement Fourier-Transform Microwave Spectrometer. *Rev. Sci. Instrum.* **1996**, *67*, 4072–4084.
- (59) Grabow, J.-U.; Stahl, W. Notizen: A Pulsed Molecular Beam Microwave Fourier Transform Spectrometer with Parallel Molecular Beam and Resonator Axes. *Z. Naturforsch.* **1990**, *45a*, 1043–1044.

- (60) Ferres, L.; Cheung, J.; Stahl, W.; Nguyen, H. V. L. Conformational Effect on the Large Amplitude Motions of 3,4-Dimethylanisole Explored by Microwave Spectroscopy. *J. Phys. Chem. A* **2019**, *123*, 3497–3503.
- (61) Zhao, Y.; Nguyen, H. V. L.; Stahl, W.; Hougen, J. T. Unusual Internal Rotation Coupling in the Microwave Spectrum of Pinacolone. *J. Mol. Spectrosc.* **2015**, *318*, 91–100.
- (62) Ohashi, N.; Hougen, J. T.; Suenram, R. D.; Lovas, F. J.; Kawashima, Y.; Fujitake, M.; Pyka, J. Analysis and Fit of the Fourier-Transform Microwave Spectrum of the Two-Top Molecule N-Methylacetamide. *J. Mol. Spectrosc.* **2004**, *227*, 28–42.
- (63) Dindić, C.; Ludovicy, J.; Terzi, V.; Lüchow, A.; Vogt, N.; Demaison, J.; Nguyen, H. V. L. Determination of the Semiexperimental Equilibrium Structure of 2-Acetylthiophene in the Presence of Methyl Internal Rotation and Substituent Effects Compared to Thiophene. *Phys. Chem. Chem. Phys.* **2022**, *24*, 3804–3815.
- (64) Ferres, L.; Stahl, W.; Nguyen, H. V. L. The Molecular Structure of Phenetole Studied by Microwave Spectroscopy and Quantum Chemical Calculations. *Mol. Phys.* **2016**, *114*, 2788–2793.
- (65) Ferres, L.; Mouhib, H.; Stahl, W.; Nguyen, H. V. L. Methyl Internal Rotation in the Microwave Spectrum of *o*-Methyl Anisole. *ChemPhysChem* **2017**, *18*, 1855–1859.
- (66) Nguyen, H. V. L.; Grabow, J. The Scent of Maibowle – π Electron Localization in Coumarin from Its Microwave-Determined Structure. *ChemPhysChem* **2020**, *21*, 1243–1248.

- (67) Kisiel, Z.; Desyatnyk, O.; Pszczółkowski, L.; Charnley, S. B.; Ehrenfreund, P. Rotational Spectra of Quinoline and of Isoquinoline: Spectroscopic Constants and Electric Dipole Moments. *J. Mol. Spectrosc.* **2003**, *217*, 115–122.
- (68) *Quantities, Units, and Symbols in Physical Chemistry*, 2nd ed.; Mills, I., IUPAC, Eds.; CRC Press: Boston, 1993.
- (69) Van, V.; Stahl, W.; Nguyen, H. V. L. The Structure and Torsional Dynamics of Two Methyl Groups in 2-Acetyl-5-Methylfuran as Observed by Microwave Spectroscopy. *Chemphyschem* **2016**, *17*, 3223–3228.
- (70) Tran, Q. T.; Errouane, A.; Condon, S.; Barreteau, C.; Nguyen, H. V. L.; Pichon, C. On the Planarity of Benzyl Cyanide. *J. Mol. Spectrosc.* **2022**, *388*, 111685.
- (71) Nygaard, L.; Asmussen, E.; Høg, J. H.; Maheshwari, R. C.; Nielsen, C. H.; Petersen, I. B.; Rastrup-Andersen, J.; Sørensen, G. O. Microwave Spectra of Isotopic Thiazoles. Molecular Structure and ^{14}N Quadrupole Coupling Constants of Thiazole. *J. Mol. Struct.* **1971**, *8*, 225–233.